Monthly Notices
of the
ROYAL ASTRONOMICAL SOCIETY

MNRAS **508,** 2937–2943 (2021)
Advance Access publication 2021 October 1

https://doi.org/10.1093/mnras/stab2763

Periodic variability of the $z = 2.0$ quasar QSO B1312+7837

M. Minev,[1,2★] V. D. Ivanov,[3] T. Trifonov,[4] E. Ovcharov,[1] S. Fabrika,[5] O. Sholukhova,[5] A. Vinokurov,[5] A. Valcheva[1] and P. Nedialkov[1]

[1]*Department of Astronomy, Faculty of Physics, University St. Kliment Ohridsky, 05 James Bourchier, 1164 Sofia, Bulgaria*
[2]*Institute of Astronomy and NAO, Bulgarian Academy of Sciences, 72 Tsarigradsko Shose Blvd., 1784 Sofia, Bulgaria*
[3]*European Southern Observatory, Karl Schwarzschildstr. 2, D-85748 Garching bei München, Germany*
[4]*Max-Plank-Institut für Astronomie, Königstuhl 17, D-69117 Heidelberg, Germany*
[5]*Special Astrophysical Observatory of the Russian Academy of Science (SAO RAS), Nizhnij Arkhyz, Karachai-Cherkessia, 369152, Russia*

Accepted 2021 September 21. Received 2021 September 20; in original form 2021 January 17

ABSTRACT

We report here the first results from a 15-yr long variability monitoring of the $z = 2.0$ quasar QSO B1312+7837. It shows luminosity changes with a period $P \sim 6.13$ yr ($P \sim 2.04$ yr at rest frame) and amplitude of ∼0.2 mag, superimposed on a gradual dimming at a rate of ∼0.55 mag per 100 yr. Two false periods associated with power peaks in the data windowing function were discarded. The measured period is confirmed with a bootstrapping Monte Carlo simulation. A damped random walk model yields a better fit to the data than a sine-function model, but at the cost of employing some high-frequency variations which are typically not seen in quasars. We consider the possible mechanisms driving this variability, and conclude that orbital motion of two supermassive black holes – result from a recent galaxy merger – is a possible explanation.

Key words: galaxies: active – quasars: individual: QSO B1312+7837 – quasars: supermassive black holes.

1 INTRODUCTION

Supermassive black holes (SMBHs) reside at the centres of massive galaxies (Wolfe & Burbidge 1970). They dominate the kinematic evolution of the central regions of galaxies, and affect the evolution of their stellar populations. During the phases of active accretion, the active galactic nucleus (AGN) phenomenon occurs, giving rise to the quasars, that are used to probe the distant Universe (Hills 1975).

Galaxies often interact with each other and their merging can form a new nucleus that contains two SMBHs (Begelman, Blandford & Rees 1980). The most direct search for binarity of SMBHs is to look for spatially resolved sources of X-ray, radio emission, or broad-line optical emission within the same host galaxy, but this is usually limited to nearby objects (NGC 6240, Mrk 212; Komossa et al. 2003; Rubinur et al. 2021) and difficult, even by interferometry (D'Orazio & Loeb 2018). However, some SMBHs can be ejected from the host galaxy – Ward et al. (2021) reported nine candidates. Double-peak lines, associated with AGNs also indicate binarity (Halpern & Filippenko 1988; Eracleous & Halpern 1994; Smith et al. 2010; Severgnini et al. 2021). Another option – adopted here – is to look for periodicity of the emission from unresolved AGNs, modulated by the orbital motion of the two SMBHs (Sillanpaa et al. 1988; Fan et al. 1998; Graham et al. 2015a; Charisi et al. 2016; Liu et al. 2016). In an extensive review, Komossa (2006) lists a few other indicators of SMBH binary: double-double radio galaxies and X-shaped radio galaxies.

Various mechanisms that cause this variability have been considered. One possibility is that the orbital motion modulates the accretion rate on the SMBHs (D'Orazio, Haiman & MacFadyen 2013). Another is a transit of the 'secondary' SMBH in front of the accretion disc of the 'primary' SMBH (Lehto & Valtonen 1996). This occurs when the distances between SMBHs are less than 1 pc, and in such cases the two components can spiral towards the common centre of mass and eventually merge (Begelman et al. 1980). The orbital motion causes strong gravitational waves that should be detectable from the latest experiments (Kelley et al. 2019), but such events are rare. The studies of SMBHs binaries are important for understanding the galaxy mergers, for nature of SMBHs themselves, and for the physics of the gravitational waves.

Here, we report the results of a long-term variability monitoring of the quasar QSO B1312+7837 ([VV2006] J131321.4+782153, WISEA J131321.33+782153.8, *Gaia* DR2 1716672593984035072; Véron-Cetty & Véron 2006) at $z = 2.0$ (Hagen, Engels & Reimers 1999). It shows the typical broad emission lines (Tytler et al. 2004). Its mean magnitude is $B \sim 16.4$ mag, corresponding to an absolute magnitude of $M_B = -30.1$ mag (Mickaelian et al. 1999), ∼3.5 mag brighter than the mean M_B for quasars at the same redshift (Souchay et al. 2015). Intranight observations with a minute-long cadence showed no short-term variability (Bachev, Strigachev & Semkov 2005).

2 OBSERVATIONS

The observations were obtained at the Rozhen National Astronomical Observatory (NAO) with a number of imagers (Table 1 and for the FoReRo-2 – in Jockers et al. 2000) equipped with standard photometric Johnsons-Cousins *UBVRI* filters. The integration times were 1.5–5 min and the seeing was 1.5–2.0 arcsec. The field around the quasar and the reference stars are shown in Fig. 1. The observing

★ E-mail: msminev@phys.uni-sofia.bg

Table 1. Observing facilities. The columns contain telescope, camera, field of view (FoV), and pixel scale.

Telescope	Camera	FoV (arcmin)	Scale (arcsec px^{-1})
50-/70-cm *Schmidt*	SBIG ST-8	27.5 × 18.3	1.08
50-/70-cm *Schmidt*	SBIG STL-11000M	72.1 × 48.1	1.08
50-/70-cm *Schmidt*	FLI PL-16803	73.7 × 73.7	1.08
2-m *Ritchey-Chretien-Coude*	VersArray 1300B	5.8 × 5.6	0.26
2-m *Ritchey-Chretien-Coude*	FoReRo-2	17.1 × 17.1	0.50

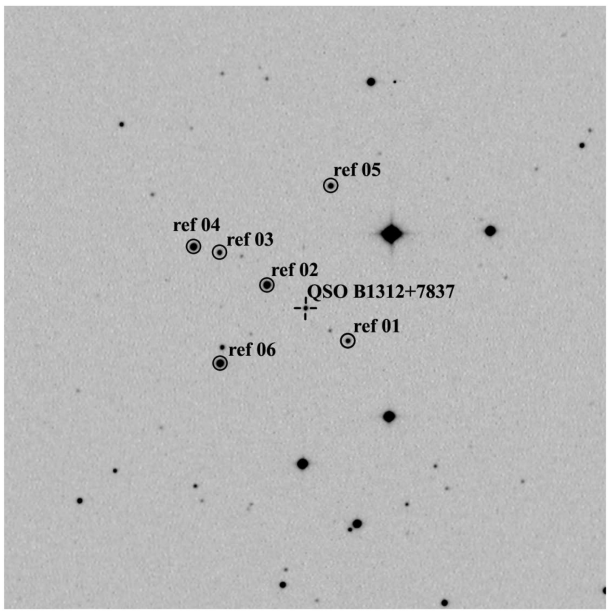

Figure 1. The field (10 × 10 arcmin) around QSO B1312+7837 (cross). The stars used as references are marked with circles. North is up, east is left.

Table 2. Photometric light curve QSO B1312+7837. Only the first five entries are shown for guidance; the entire table is available in the electronic edition of the journal. The columns contain: Julian date, standard *R*-band magnitude, and its error for the quasar and two reference stars.

JD−245 3000	QSO *R* (mag)	Error (mag)	Ref-01 *R* (mag)	Error (mag)	Ref-05 *R* (mag)	Error (mag)
494.350	15.942	0.083	15.558	0.082	15.099	0.082
494.500	15.922	0.078	15.557	0.078	15.107	0.077
623.325	16.037	0.020	15.655	0.019	15.190	0.019
624.335	16.035	0.017	15.673	0.015	15.202	0.014
626.460	16.041	0.019	15.659	0.018	15.208	0.017

campaign starts from JD 2453494 and the quasar's apparent *R*-band magnitudes are in range of 15.89–16.20 mag with typical photometric error 0.01–0.04 mag. A sample of the photometric data of the quasar and two reference stars (ref-01 – USNOA2 1650-01631981 and ref-05 – USNOA2 1650-01632068) is show in Table 2 and the entire data are available in the electronic edition of the journal. There is no evidence for variability of these two stars (Henden et al. 2016) and as we can see from our observations their magnitude is constant in time. Comparison between magnitudes of any of these stars and the quasar shows variability that cannot be produced by some correlated image noise or the different observational equipment.

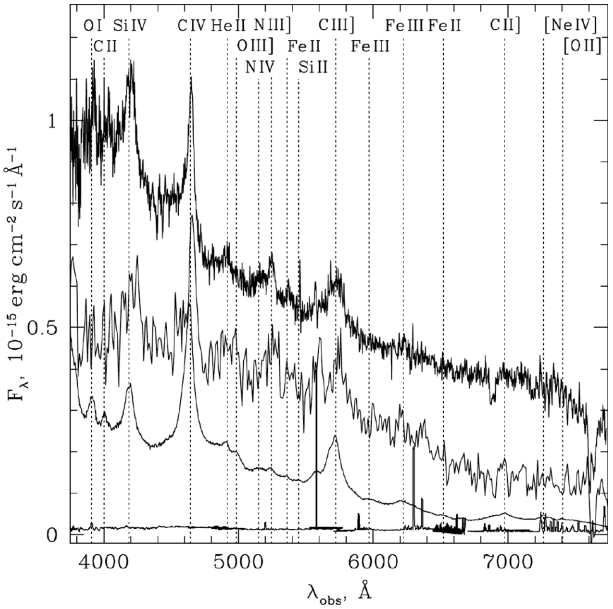

Figure 2. Optical spectra at observed wavelengths of (from top to bottom): QSO B1312+7837 from the 6-m *BTA* telescope and from the 2.2-m telescope on Calar Alto (shifted down by 0.3 for display purposes; Hagen et al. 1999), a combined SDSS (Sloan Digital Sky Survey) quasar spectrum shifted to $z = 2$ (Vanden Berk et al. 2001) and a sky spectrum. Some prominent quasar emission features are marked.

The data were processed with the IRAF (Tody 1986, 1993)[1] and included the usual steps: bias/dark subtraction, flat-fielding, and flux calibration. Aperture photometry was performed using the `APPHOT IRAF` package. The images were flux calibrated with standards from Stetson (2000). To exclude variable sources, we considered only stars with rms ≤ 0.2 mag. For the VersArray 1300B data, we applied an additional correction to remove a known radial flux variation (Ovcharov et al. 2008).

A spectrum of QSO B1312+7837 was obtained on 2018 Feb 18, at the 6-m BTA (Bolshoi Teleskop Altazimutalny) telescope at the *Special Astrophysical Observatory* with SCORPIO (Spectral Camera with Optical Reducer for Photometric and Interferometrical Observations; Afanasiev & Moiseev 2005), equipped with 2048 × 2048 EEV 42-40 detector, yielding a FOV of 6.1 arcmin on the side. The slit was 1-arcsec wide and the volume phase holographic grating VPHG550G was used, delivering a resolving power $R \approx 550$ and full width at half-maximum = 10 Å over a wavelength range 3700−7700 Å. The integration time was 3000 sec (5 × 600 sec exposures). The data processing included bias/dark subtraction, flat-fielding, extraction, wavelength calibration, and a flux calibration. The final spectrum is shown in Fig. 2.

We measured a redshift 1.999 ± 0.004 for N V 1240, Si IV 1394, Si IV 1403, C IV 1549, He II 1640, Ne III 1750, and C III] 1909 lines. It is indistinguishable from the value of Hagen et al. (1999). The error was determined as in Ivanov et al. (2016), as a standard deviation of the redshifts measured from the seven lines – with the caveat that the standard deviation for a small number of measurements is not well defined, but we based this estimate only on relatively strong and isolated lines, without apparent intervening absorptions.

[1]IRAF is distributed by the *National Optical Astronomy Observatory*, which is operated by the Association of Universities for Research in Astronomy under a cooperative agreement with the National Science Foundation.

3 ANALYSIS

3.1 Period search

For quasar periodicity search, we used a modified version of the `Exo-Striker` tool (Trifonov 2019), which provides easy access to a large variety of algorithms for time-series analysis. To search for periodic signals in the photometry, we first constructed a generalized Lomb–Scargle (GLS; Zechmeister & Kürster 2009) power spectrum periodogram on the Rozhen NAO *R*-magnitude data, which have the longest temporal baseline and best quality. We adopted a false alarm probability (FAP), a significance threshold of 10^{-3} (0.1 per cent), and we inspected the frequency range between one day and two times the length of the observations' temporal baseline, which is 5485 d. For our GLS periodogram tests, we always included a white-noise model. The variance is quadratically added to the error budget of the *R*-magnitude data. Additionally, we perform a discrete fast Fourier analysis of the Rozhen NAO *R*-magnitude data to study the window function (WF) of the data, affecting our period search.

Fig. 3 shows the results from our WF and GLS periodicity search test. The top panel of Fig. 3 shows WF power, which shows many peaks. The strongest is at 4388 d and there is another one at 29.5 d that is close to the Lunar synodic month, affecting the observational schedule. The middle panel of Fig. 3 shows the GLS periodogram of the Rozhen NAO *R*-magnitude data. We found two very significant GLS peaks: at a period of 2307.6 d (FAP $< 10^{-49}$), and another at a period of 6254.6 d (FAP $< 10^{-58}$) centred at a broad, low-frequency power structure. However, the latter has a longer period than the temporal baseline, thus it is not a firm detection. An adequate explanation of the significant low-frequency GLS power is the presence of a signal component, which cannot be resolved on our limited temporal baseline. Indeed, a visual inspection of the all filters photometric data suggests a gradual magnitude decline. This motivated us to apply a linear trend fit to the NAO *R*-magnitude data, which confirmed the presence of a significant photometric magnitude decline (see Section 3.2). The bottom panel of Fig. 3 shows the GLS periodogram of the best-fitting residuals of the linear trend model. We still find two significant low-frequency signals. Compensating the brightness decay, reduced the power and the period of the lowest frequency signal, which is now detected near ∼4660 d, whereas the second strongest peak in the raw *R*-band photometry is now the most significant peak, but with a slightly different period at 2214.4 d. In addition, we find evidence of a strong GLS period near ∼29 d. We find, however, that the 4660.34- and the 29.32-d signals are most likely related to the aliases of the WF and the true period of 2214.42 d. Indeed, $P_{\rm alias\,1} = 1/(f_{\rm WF=29.5\,d} - f_{2214\,\rm d}) \approx 29.6$ d and $P_{\rm alias\,2} = 1/(f_{2214.4} - f_{\rm WF=4388\,d}) \approx 4500$ d. Therefore, we concluded that the periodic signal evident in the data is at a period near 2214 d, whereas the remaining strong power in the GLS power is likely induced by a combination of an additional photometric variability of unknown nature that appears as a linear trend, and the WF aliasing with the true period.

3.2 Parameter optimization and model selection

We adopted the SIMPLEX algorithm (Nelder & Mead 1965), which optimizes the negative logarithm of the likelihood function ($-\ln \mathcal{L}$), coupled with three competing models: (i) a 'null' model assuming no signal in the data; (ii) a sinusoidal model where the optimized parameters are the photometric signal, amplitude, phase, and period; and (iii) a sinusoidal model as (ii), but with an additional linear brightness decline term. For models (ii) and (iii), we adopted the

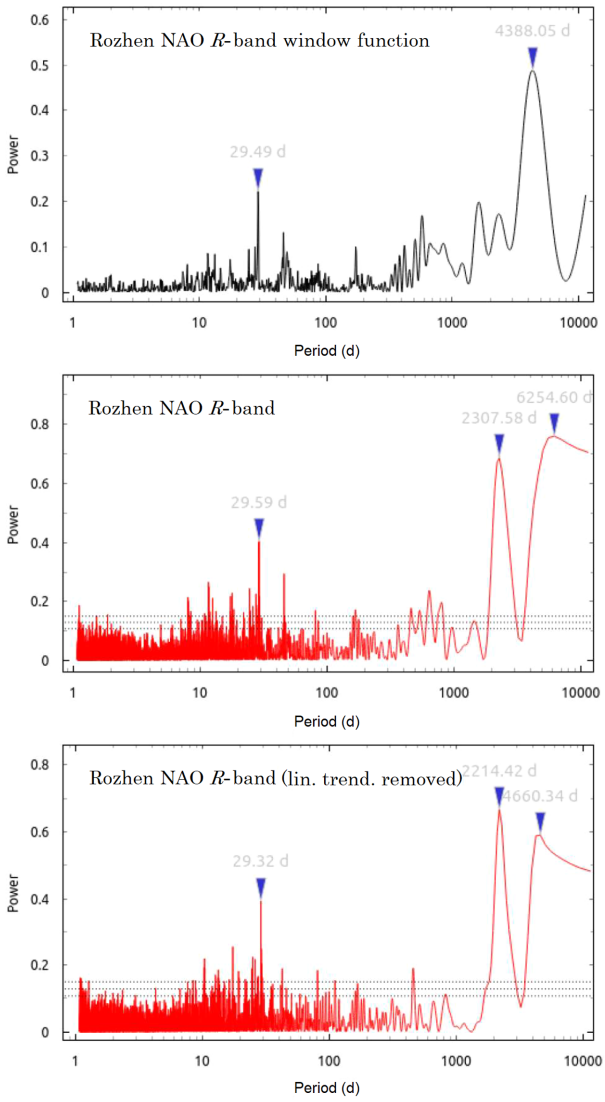

Figure 3. Top panel: WF power spectrum of the Rozhen NAO *R*-band photometry for QSO B1312+7837. The observational scheduling induces strong WF power at periods of 29.49 d, and 4388.05 d, among others. Middle panel: GLS power spectra of the Rozhen NAO *R* band. Horizontal dashed lines indicate the FAP thresholds of 10, 1, and 0.1 per cent. The three most significant powers are at periods 29.59, 2307.58, and 6254.60 d. Bottom panel: Same as the panel above, but after a linear trend model is subtracted from the *R*-band photometry. The true period is near 2214.42 d, whereas the 4660.34 and 29.32 d are its aliases of the WF peaks at periods of 4388.05 and 29.59 d, respectively.

2214.4-day peak, phase, and amplitude estimate from the GLS analysis as an initial guess for parameter optimization. Additionally, for all models we vary the nuisance parameters: the mean 'offset' of the photometric data, and the white-noise variance term, which we add in quadrature to the nominal *R*-band uncertainties while fitting (i.e. a data 'jitter' term, see Baluev 2009). For posterior analysis, we ran an affine-invariant ensemble Markov chain Monte Carlo (MCMC) sampler (Goodman & Weare 2010) via the `emcee` package (Foreman-Mackey et al. 2013). We adopted non-informative flat priors of the parameters, and we explored the parameter space starting from the best-fitting parameters returned by the SIMPLEX minimization. We ran 100 independent walkers in parallel adopting 1000 'burn-in' MCMC steps, which we discard from the analysis,

followed by 5000 MCMC steps, from which we constructed the posterior parameter distribution. We evaluate the acceptance fraction of the `emcee` sampler, which as recommended by Goodman & Weare (2010), should be between 0.2 and 0.5, to consider whether the MCMC chains have converged. We adopted the 68.3 per cent confidence intervals of the MCMC posterior distributions as a 1σ uncertainty estimate of the parameters.

The best-fitting statistical properties of three competing models in terms of Bayesian information criteria[2] (BIC) are as follows: $BIC_{\rm flat} = -414.98$, $BIC_{\rm Sine} = -618.25$, and $BIC_{\rm Sine+trend} = -739.37$. With a $\Delta BIC = BIC_{\rm flat} - BIC_{\rm Sine+trend} = 324.39$, represents a very strong evidence in support of the quasar periodic variability. Our final results derived a quasar variability with a period of 2237 ± 12 d (corresponding to 746 ± 4 d at frame of rest). The light curve is shown in Fig. 4.

As a consistency check, we carried out an independent analysis fitting the observational light curve with a combination of a sinusoidal and a linear trend. To estimate the errors of the derived parameters we carried out a semi-empirical Monte Carlo bootstrapping simulation, following Cáceres et al. (2009, 2011): After we obtain the best fit for the $i^{\rm th}$ observation, we calculate the deviation from the best fit and then we add this deviation to the $(i{+}1)^{\rm th}$ observation. In a circular fashion, the deviation for the last observation is added to the first observation. Thus, we create a new sample and repeat the fit. In the next step, we add the deviation for the $i^{\rm th}$ observation to the $(i{+}2)^{\rm th}$ observation, and re-fit, until we have created a number of realizations equal to the number of observations minus one. A drawback of this method is that the number of realizations is limited by the number of observations but the procedure preserves any systematic effects that may be present in the data: If there is a cluster of measurements with larger errors, e.g. because there was a batch of adjacent night with poor weather conditions, this structure will be preserved in the simulation and will contribute in the same systematic way to the uncertainties of the derived parameters. The results are listed in Table 3 and they agree, within the errors with the `Exo-Striker` analysis.

3.3 Stochastic variability and damped random walk model

It has been suggested in the literature that quasars' optical variability could be well explained with red-noise stochastic processes instead of other physical phenomena such as close binary SMBH (see e.g. Kelly et al. 2009; Kozlowski et al. 2010; MacLeod et al. 2010). In this context, it is essential to test the probability of the optical variability of QSO B1312+7837 being a true periodicity rather than a manifestation of correlated red noise. A commonly used stochastic process for modelling optical variability in quasars is the damped random walk (DRW) model (Kelly et al. 2009), which could be tested against our periodic best fit presented in Section 3.2.

For the purpose, we adopted the `RealTerm` Gaussian process (GP) regression kernel intrinsic to the `celerite` PYTHON package (Foreman-Mackey et al. 2017), which is included in the `Exo-Striker`. By definition, this model is a DRW process of the form: $\kappa(\tau) = a_j e^{-c_j \tau}$, where a is a amplitude and c defines the characteristic time-scale of the GP, therefore, suitable for our needs. For consistency with our best-fitting periodic model, the a and c GP hyperparameters are fitted together the mean offset and the white-noise variance nuisance parameters of the R-band data. Thus, the DRW model, and our best-fitting periodic model are nested within the null model,which assumes no periodicity.

For completeness, we also performed DRW fits with a linear trend component, and with a sine-model component, which includes a linear trend. Thus way, the DRW covariance in the likelihood function allowed us to test if it is statistically worthy of the involvement of

[2] *BIC* is defined as $-2 \times \ln \mathcal{L} + k \times \ln(N)$, where k is the number of free parameters in the model, and N is the number of data. Two competing models with different k can be tested via their ΔBIC, which must be over 10 to support the more complex model.

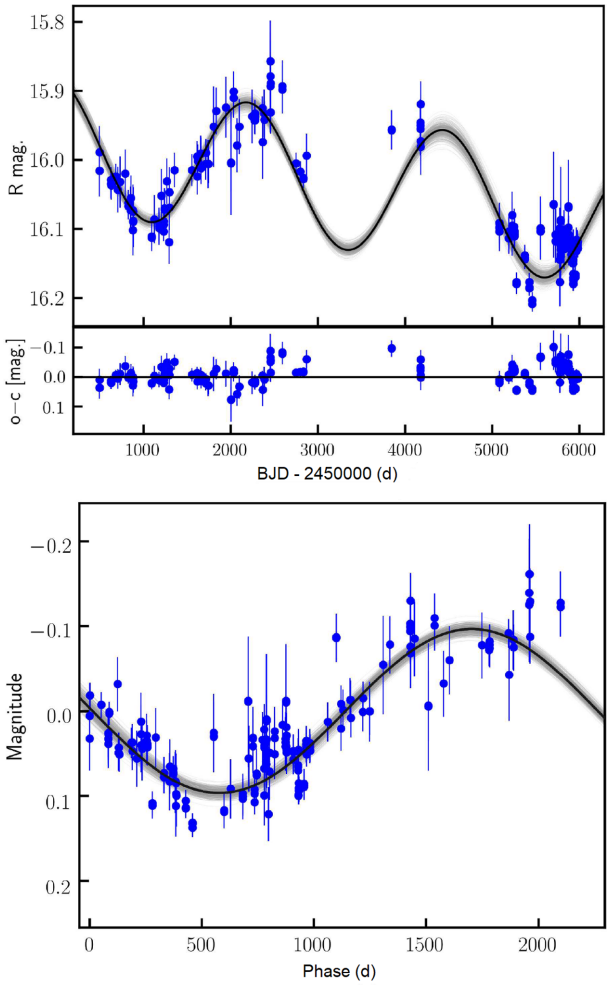

Figure 4. The top panel shows the best `Exo-Striker` fit (black) to the R-band observed data (blue) on the first panel, and residuals on the second panel. The fit is composed of strictly periodic component and a brightest decline term, which represents the data well. The bottom panel shows a period-folded R-band light curve. The shaded area is composed of 500 randomly chosen fits from the MCMC test, which visually represents the $1\,\sigma$ uncertainties of the model.

Table 3. Results from the Monte Carlo simulation.

Parameter	Mean	Median	Standard deviation
Sin amplitude (mag)	0.095	0.098	0.010
Sin period (d)	2248.2	2253.3	53.1
Sin phase (d)	−1.45	−1.43	0.28
Linear slope (mag^{-1} d)	1.52e-05	1.51e-05	0.40e-05
Average magnitude (mag)	15.977	15.974	0.014
rms (mag)	0.0065	0.0062	0.0017

a liner, periodic, or both components beyond the possible correlated DRW variations.

We achieved DRW parameters estimates of $a = 0.0058^{+0.0017}_{-0.0001}$, and $c = 0.0015^{+0.0002}_{-0.0011}$, leading to a low rms = 0.0117 mag, and $BIC_{\rm DRW}$ = −849.54. With $\Delta BIC = BIC_{\rm Sine+trend} - BIC_{\rm DRW} = 110.17$, this gives a significant advantage to the DRW model with respect to our adopted periodic model. The addition of a linear trend to the DRW model decreased the BIC evidence to $BIC_{\rm DRW+trend} = -847.49$, which means that assuming we observe stochastic processes in our data, the addition of this parameter is not well justified. The inclusion of a periodic component to the latter model, however, gives a better $BIC_{\rm DRW+Sine+trend} = -853.22$. This leads to positive evidence of $\Delta BIC = 3.68$ with respect to the DRW-only model, which means that the NAO-Rozhen data of QSO B1312+7837 could indeed be consistent with a periodic behaviour under the assumption that we pre-dominantly observe correlated red-noise variations.

We concluded that the DRW + Sine + linear trend model is by far the best model, although only marginally better than a simpler DRW-only model. Fig. 5 shows the DRW best-fitting models and their computed GP covariance in addition to Fig. 4, which shows our best periodic model. Indeed, a visual inspection of the DRW residuals in Fig. 5 suggests nearly perfect agreement with the DRW models. Can then red-noise stochastic processes explain the optical variability of QSO B1312+7837?

While we cannot reject this possibility, we warn that our DRW model has at least a few major caveats. First, the DRW model is consistent with high-frequency behaviour, which has a strong tendency to overfit data. In this context, the DRW model would be adequate only if we have strong priors on the stochastic processes in quasars, which could constrain a and c. Second, a direct comparison between a simple strictly periodic Sine model composed of linear parameters[3] and a highly flexible GP model with two hyperparameters is difficult. Fair model compassion can be performed using Bayesian evidence analysis based on parameter posterior distribution probabilities, but once again, this requires informative parameter priors of the GP, which we do not have. Finally, as Kozlowski (2017) found, the temporal baseline of the observations must be at least 10 times longer than the true DRW decorrelation time-scale. However, the characteristic correlation time-scale of our DRW model is $\approx 660^{+1800}_{-80}$ d, while we have a temporal baseline of only ∼15 yr, which is insufficient for conclusive DRW results.

Therefore, we find that the DRW model is likely inappropriate to describe our data despite the relatively good fit properties. We conclude that more credibility to the DRW possibility of QSO B1312+7837 is possible only if more optical photometry data are collected, but that would require a few decades of observations.

3.4 Binary SMBH model: physical parameters

The spectrum allows us to estimate the two SMBH masses from for the width of the broad C IV 1549.06 Å component and the continuum luminosity at 1350 Å from Vestergaard & Peterson (2006; equations 2 and 4). Two scenarios must be considered here. First, if the separation between the two SMBHs is wide, so each has its own accretion disc, and the orbital motion of the SMBHs around their common centre of masses does not contribute significantly to the width of the emission lines, then the final mass will be the luminosity-weighted average of the masses of the two SMBHs. Second, if the SMBHs are close in, and are immersed into a single accretion disc, we will obtain from the width of the broad emission lines an upper limit to the combined mass of the two SMBHs, because the motion of the binary SMBHs is expected to produce additional widening of the emission lines. We cannot distinguish between the two options and can only conclude that the combined mass of the two SMBHs must be lower than twice the obtained estimate.

Given the resolution of our spectra, the deblending of the narrow and the broad C IV components gives uncertain results. We performed it with the IRAF task *splot* and obtained widths of 2700 ± 200 and 9700 ± 600 km s^{-1}, respectively. The relation of Vestergaard & Peterson (2006) yields an estimate of $\log(M_{\rm BH}/{\rm M}_\odot)$ ∼8.1 ± 0.1 which, as discussed above, implies that the combined mass of the two SMBHs in the system cannot exceed twice this value.

Assuming a circular orbit, for the derived rest frame period, a mass ratio of the two black holes between 0.5 and 1, and masses in the generously wide range $\log(M_{\rm BH}/{\rm M}_\odot)$ ∼8–8.6, we obtain orbital velocity for the primary SMBH in the range of 3600–8600 km s^{-1} and for the secondary companion – of 5500–11500 km s^{-1}, following D'Orazio, Haiman & Schiminovich (2015b). This is ∼1–4 per cent of the speed of light, sufficient to cause relativistic boost.

The flux change caused by Doppler boosting of a power-law spectrum $F_\nu \sim \nu^\alpha$ is $F^{\rm max}/F^{\rm min} = ((1+\beta \sin i)/(1-\beta \sin i))^{(3-\alpha)}$ (e.g. Pelling et al. 1987; Dubus, Cerutti & Henri 2010). From our spectrum, after a correction for Milky Way reddening using the extinction law of Cardelli, Clayton & Mathis (1989) and $A_V \sim 0.09$ mag from Schlafly & Finkbeiner (2011), we measured an average slope $\alpha = -0.24 \pm 0.05$ over λ ∼1400–2600 Å. The slope error is tentatively adopted conservative value: the formal fitting error is typically 0.02–0.03, but the slope varies within ∼0.05 depending on the wavelength range and the masking of the emission lines. We carried out the same analysis of the archival spectrum from Hagen et al. (1999) and obtained similar slope. To explain, the observed $F^{\rm max}/F^{\rm min} \sim 0.2$ this implies that the line-of-sight velocity needs to be $v \sin i \sim 8550$ km s^{-1}, at the limit of the orbital velocity for the primary black hole, but well within the range of orbital velocity for the secondary.

For the mass range and the derived period the Kepler's third law yields a semimajor axis of 0.008–0.012 pc which is significantly larger than the innermost marginally stable circular orbit for SMBHs within the considered mass range: $r_{ISCO} \sim 10^{-4}$–10^{-5} (for a SMBH with spin $a = 0$ or even six times smaller for a SMBH with spin $a = 1$; Tanaka & Menou 2010).

To place QSO B1312+7837 in broader context we compare the physical parameters we derived for this object with the parameters of quasars in the MacLeod et al. (2010) sample. For apparent i magnitude 16.052 ± 0.005 mag (Chambers et al. 2016) and adopting a cosmological model with $H_0 = 70.0$ km s^{-1} Mpc^{-1} and $\Omega_M = 0.3$, yielding a distance modulus of ∼45.95 mag[4] we obtain $M_i \sim -29.9$ mag placing QSO B1312+7837 at the brightest end of the quasar locus – this is expected for quasars at higher redshift but it also hints that the true black hole mass of QSO B1312+7837 is more likely to be closer to the upper end of our mass range (fig. 12 in MacLeod et al. 2010).

4 DISCUSSION AND CONCLUSIONS

The binary SMBHs evade detection for a number of reasons: because the velocity difference is smaller than the intrinsic width of the

[3]The period P is a non-linear parameter, but is strongly constrained by the GLS test.

[4]https://cosmocalc.icrar.org/

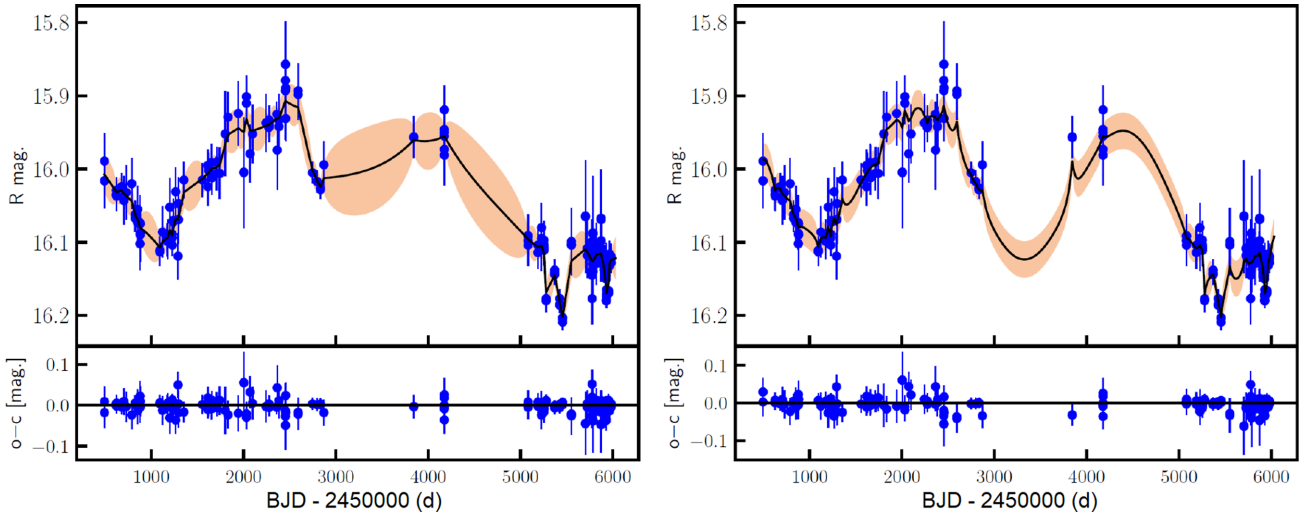

Figure 5. Same as top panel of Fig. 4, but for an alternative DRW GP model with a linear trend (left-hand panel), and a DRW GP model with a linear trend and a periodic component (right-hand panel). The black solid curve shows the best-fitting model, whereas the computed GP covariance is shown with orange. The residuals are shown on the lower subpanels.

emission lines or because the offset nuclei are too close to be resolved with the existing instrumentation etc. Other techniques require competitive observing time at the few X-ray missions or moderately high-resolution high-multiplexity vast spectroscopic surveys. On the other hand, the new or soon to enter operation all sky variability monitoring projects like Pan-STARRS and LSST/VRO (Kaiser et al. 2002; Ivezić et al. 2019) will make the demographic studies of binary SMBHs more accessible.

The masses of quasars were first estimated with arguments related with their bolometric luminosities (Soltan 1982). The reverberation mapping (Blandford & McKee 1982) provided more accurate estimates and the scaling relations with the bulge properties (Ferrarese & Merritt 2000; Gebhardt et al. 2000) allowed for studies of SMBH demographics. The vast majority of SMBHs have masses in the range $\log(M_{\rm BHs}/{\rm M}_{\odot})$ ∼7–9 (Marconi et al. 2004), with low- and high-record holders of $\log(M_{\rm BHs}/{\rm M}_{\odot})$ ∼5 and 11 (López-Cruz et al. 2014; Baldassare et al. 2015). Our upper mass limit is well within this range.

The estimated orbital elements make QSO B1312+7837 similar to PG 1302−102, a well-known subpc separation quasar with $z = 0.3$ that shows sinusoidal variations in the optical (Graham et al. 2015b; D'Orazio et al. 2015b). However, straightforward interpretation of the observed period and all other related properties is hampered by the unknown mass ratio of the two SMBH components and the decoupling between the SMBH orbital period and the strongest periodicity in the accretion rate on to the SMBHs – D'Orazio et al. (2015a) pointed out that the latter may correspond to the orbital period of accreted gas at a distance of a few binary separations. Therefore, the binary SMBH might be much tighter than suggested by the 2-yr rest-frame period, and even be in the gravitational wave-dominated orbital decay regimen. X-ray spectroscopy of features formed in the innermost region of the accretion disc may offer the only opportunity to probe directly the SMBH orbit, their mass ratio, and the dominant orbital decay mechanism. Finally, if the Doppler boosting account for the flux modulation, the calculated orbital velocities imply that the majority of the emission probably originates around the secondary component, because the observed amplitude can only be accounted for with velocities at the limit of the velocity range for the primary.

We note that the sinusoidal light curve can be explained by other models, including the presence of a hotspot in the inner accretion disc or a warp in the disc itself (Graham et al. 2015a). It is still possible that periodic variations in the light curves of quasars could be a manifestation of correlated 'red-noise' stochastic systematics. For example, Vaughan et al. (2016) also studied the light curve of PG 1302−102, and found that stochastic 'red-noise' processes are likely preferred over a sinusoidal variation. For precise stochastic process analyses of QSO B1312+7837, we need longer baseline observations with high cadence to provide accurate results from the models.

Summarizing, we found a variation with a probable period of 2214 ± 12 d in the apparent brightness of the $z = 2.0$ QSO B1312+7837. This modulation can be described with a binary SMBH with a combined upper mass limit of $\log(M_{\rm BHs}/{\rm M}_{\odot})$ $\sim 8.4 \pm 0.1$ – a value that places this object within the typical SMBH mass range. We argue that the advent of all-sky synoptic surveys will soon allow carrying out studies of the SMBHs demographics.

ACKNOWLEDGEMENTS

We thank to Zhang-Liang Xie for very useful discussion, and for confirming our DRW results using `JAVELIN` code (Zu et al. 2013). We acknowledge support by Bulgarian NSF (National Science Fund) under grant DN18-10/2017 and National RI Roadmap Projects DO1-277/16.12.2019 and DO1-268/16.12.2019 of the Ministry of Education and Science for the Republic of Bulgaria. We report to study RFBR (Russian Foundation for Basic Research) project no. 19-02-00432. TT acknowledges support by the DFG (German Research Foundation) Research Unit FOR 2544: *Blue Planets around Red Stars*. Observations with the *SAO RAS* telescopes are supported by the Ministry of Science and Higher Education of the Russian Federation (including agreement no. 05.619.21.0016, project ID RFMEFI61919X0016). Optical spectroscopy of the sources was performed as part of the government contract of the *SAO RAS* approved by Ministry of Science and Higher Education of the Russian Federation. The authors thank the anonymous referee for the useful comments.

This study is based on observations gathered at Rozhen National Astronomical Observatory.

DATA AVAILABILITY

The data underlying this article are available in the article and in its online supplementary material.

REFERENCES

Afanasiev V. L., Moiseev A. V., 2005, Astron. Lett., 31, 194
Bachev R., Strigachev A., Semkov E., 2005, MNRAS, 358, 774
Baldassare V. F., Reines A. E., Gallo E., Greene J. E., 2015, ApJ, 809, L14
Baluev R. V., 2009, MNRAS, 393, 969
Begelman M. C., Blandford R. D., Rees M. J., 1980, Nature, 287, 307
Blandford R. D., McKee C. F., 1982, ApJ, 255, 419
Cáceres C. et al., 2011, A&A, 530, A5
Cáceres C., Ivanov V. D., Minniti D., Naef D., Melo C., Mason E., Selman F., Pietrzynski G., 2009, A&A, 507, 481
Cardelli J. A., Clayton G. C., Mathis J. S., 1989, ApJ, 345, 245
Chambers K. C. et al., 2016, preprint (arXiv:1612.05560)
Charisi M., Bartos I., Haiman Z., Price-Whelan A. M., Graham M. J., Bellm E. C., Laher R. R., Márka S., 2016, MNRAS, 463, 2145
D'Orazio D. J., Haiman Z., MacFadyen A., 2013, MNRAS, 436, 2997
D'Orazio D. J., Haiman Z., Duffell P., Farris B. D., MacFadyen A. I., 2015a, MNRAS, 452, 2540
D'Orazio D. J., Haiman Z., Schiminovich D., 2015b, Nature, 525, 351
D'Orazio D. J., Loeb A., 2018, ApJ, 863, 185
Dubus G., Cerutti B., Henri G., 2010, A&A, 516, A18
Eracleous M., Halpern J. P., 1994, ApJS, 90, 1
Fan J. H., Xie G. Z., Pecontal E., Pecontal A., Copin Y., 1998, ApJ, 507, 173
Ferrarese L., Merritt D., 2000, ApJ, 539, L9
Foreman-Mackey D., Hogg D. W., Lang D., Goodman J., 2013, PASP, 125, 306
Foreman-Mackey D., Agol E., Ambikasaran S., Angus R., 2017, AJ, 154, 220
Gebhardt K. et al., 2000, ApJ, 539, L13
Goodman J., Weare J., 2010, CAMCS, 5, 65
Graham M. J. et al., 2015a, MNRAS, 453, 1562
Graham M. J. et al., 2015b, Nature, 518, 74
Hagen H.-J., Engels D., Reimers D., 1999, A&AS, 134, 483
Halpern J. P., Filippenko A. V., 1988, Nature, 331, 46
Henden A. A., Templeton M., Terrell D., Smith T. C., Levine S., Welch D., 2016, AAVSO Photometric All Sky Survey (APASS) DR9, II/336/apass9
Hills J. G., 1975, Nature, 254, 295
Ivanov V. D. et al., 2016, A&A, 588, A93
Ivezić Ž. et al., 2019, ApJ, 873, 111
Jockers K. et al., 2000, Kinematika Fiz. Nebesnykh Tel, 3, 13
Kaiser N. et al., 2002, in Tyson J. A., Wolff S., eds, Proc. SPIE Conf. Ser. Vol. 4836, Survey and Other Telescope Technologies and Discoveries, Vol. 4836. SPIE, Bellingham, p. 154
Kelley L. Z., Haiman Z., Sesana A., Hernquist L., 2019, MNRAS, 485, 1579
Kelly B. C., Bechtold J., Siemiginowska A., 2009, ApJ, 698, 895
Komossa S., 2006, Mem. Soc. Astron. Ital., 77, 733
Komossa S., Burwitz V., Hasinger G., Predehl P., Kaastra J. S., Ikebe Y., 2003, ApJ, 582, L15
Kozlowski S., 2017, A&A, 597, A128
Kozlowski S. et al., 2010, ApJ, 708, 927
Lehto H. J., Valtonen M. J., 1996, ApJ, 460, 207
Liu T. et al., 2016, ApJ, 833, 6
López-Cruz O., Añorve C., Birkinshaw M., Worrall D. M., Ibarra-Medel H. J., Barkhouse W. A., Torres-Papaqui J. P., Motta V., 2014, ApJ, 795, L31
MacLeod C. L. et al., 2010, ApJ, 721, 1014
Marconi A., Risaliti G., Gilli R., Hunt L. K., Maiolino R., Salvati M., 2004, MNRAS, 351, 169
Mickaelian A. M., Gonçalves A. C., Véron-Cetty M. P., Véron P., 1999, Afz, 42, 5
Nelder J. A., Mead R., 1965, Comput. J., 7, 308
Ovcharov E. P., Nedialkov P. L., Valcheva A. T., Ivanov V. D., Tikhonov N. A., Stanev I. S., Kostov A. B., Georgiev Ts. B., 2008, MNRAS, 386, 819
Pelling R. M., Paciesas W. S., Peterson L. E., Makishima K., Oda M., Ogawara Y., Miyamoto S., 1987, ApJ, 319, 416
Rubinur K., Kharb P., Das M., Rahna P. T., Honey M., Paswan A., Vaddi S., Murthy J., 2021, MNRAS, 500, 3908
Schlafly E. F., Finkbeiner D. P., 2011, ApJ, 737, 103
Severgnini P. et al., 2021, A&A, 646, A153
Sillanpaa A., Haarala S., Valtonen M. J., Sundelius B., Byrd G. G., 1988, ApJ, 325, 628
Smith K. L., Shields G. A., Bonning E. W., McMullen C. C., Rosario D. J., Salviander S., 2010, ApJ, 716, 866
Soltan A., 1982, MNRAS, 200, 115
Souchay J. et al., 2015, A&A, 583, A75
Stetson P. B., 2000, PASP, 112, 925
Tanaka T., Menou K., 2010, ApJ, 714, 404
Tody D., 1986, Proc. SPIE Conf. Ser. Vol. 627, Instrumentation in Astronomy VI. SPIE, Bellingham, p. 733
Tody D., 1993, in Hanisch R. J., Brissenden R. J. V., Barnes J., eds, ASP Conf. Ser. Vol. 52, Astronomical Data Analysis Software and Systems II. Astron. Soc. Pac., San Francisco, p. 173
Trifonov T., 2019, Astrophysics Source Code Library, record ascl:1906.004
Tytler D., O'Meara J. M., Suzuki N., Kirkman D., Lubin D., Orin A., 2004, AJ, 128, 1058
Vanden Berk D. E. et al., 2001, AJ, 122, 549
Vaughan S., Uttley P., Markowitz A. G., Huppenkothen D., Middleton M. J., Alston W. N., Scargle J. D., Farr W. M., 2016, MNRAS, 461, 3145
Véron-Cetty M.-P., Véron P., 2006, A&A, 455, 773
Vestergaard M., Peterson B. M., 2006, ApJ, 641, 689
Ward C. et al., 2021, ApJ, 913, 102
Wolfe A. M., Burbidge G. R., 1970, ApJ, 161, 419
Zechmeister M., Kürster M, 2009, A&A, 496, 577
Zu Y., Kochanek C. S., Kozlowski S., Udalski A., 2013, ApJ, 765, 106

SUPPORTING INFORMATION

Supplementary data are available at *MNRAS* online.

Table 2. Photometric light curve QSO B1312+7837.

Please note: Oxford University Press is not responsible for the content or functionality of any supporting materials supplied by the authors. Any queries (other than missing material) should be directed to the corresponding author for the article.

This paper has been typeset from a TEX/LATEX file prepared by the author.